



Universiteit
Leiden
The Netherlands

Complex processes in simple ices : laboratory and observational studies of gas-grain interactions during star formation

Öberg, K.I.

Citation

Öberg, K. I. (2009, September 16). *Complex processes in simple ices : laboratory and observational studies of gas-grain interactions during star formation*. Retrieved from <https://hdl.handle.net/1887/13995>

Version: Not Applicable (or Unknown)
License: [Leiden University Non-exclusive license](#)
Downloaded from: <https://hdl.handle.net/1887/13995>

Note: To cite this publication please use the final published version (if applicable).

11

PHOTOCHEMISTRY IN H₂O:CO₂:NH₃:CH₄ ICE MIXTURES

Photochemistry in NH₃-containing ices provides a potential formation pathway to amino acids and other prebiotically interesting molecules during star formation. Quantifying this UV-induced ice chemistry *in situ* has so far failed for realistic astrophysical ice analogues because of a multitude of photoproducts with overlapping infrared spectral features. While such an analogue is included in this study, the focus is instead on the spectroscopic quantification of the photochemistry at 20 K in a number of binary ice mixtures containing H₂O, CO₂, NH₃ and/or CH₄. This allows us to acquire a general understanding of branching ratios and diffusion of radicals in ices, which can be subsequently applied to more complex ice mixtures. The production of C₂H₆, C₂H₄, N₂H₄, CO, CO₃, O₃, CH₃NH₂, HCN, CH₃OH, H₂CO, CH₃CH₂OH, CH₃CHO and OCN⁻ are quantified during UV irradiation, revealing a clear difference between species that form directly from reactions between first generation radicals and species forming from later generation products. From the different formation rates of C₂H₆ and C₂H₄, the contested CH₄ photodissociation CH₃:CH₂ branching ratio is determined to be 3:1. The photochemistry in H₂O-poor and H₂O-rich ice mixtures differs because of the stronger binding environment in H₂O-rich ices, which increases the importance of relative diffusion barriers of radicals. Acid-base chemistry is found to be important in all NH₃:CO₂ containing ices; it increases the effective photodestruction cross section of NH₃ ice by up to an order of magnitude because of proton transfer from other photoproducts. Acid-base chemistry also increases the desorption temperatures of the products. To constrain the formation of glycine and other similarly complex products, TPD experiments following UV irradiation of NH₃-containing ice mixtures are presented for the first time, which confirms that amino acids and amino acid-like molecules form during photolysis of CH₄:NH₃:CO₂ ice mixtures. A complete model and a set of experiments at different temperatures are needed to further constrain different diffusion barriers and thus to model the production of complex molecules, including amino acids, in space based on specific elementary reactions.

Öberg et al. in preparation

11.1 Introduction

The molecules of life, DNA, RNA and proteins, are built up from amino acids and sugars. Pre-biotic production pathways of sugars and different nitrogen-bearing organic molecules are thus of considerable interest and a necessary component of different origin-of-life scenarios. The recent discovery of CH₃CH₂OCHO and C₃H₇CN towards Sagittarius B2(N) is indicative of an efficient formation pathway to organic molecules of comparable complexity to the smallest amino acids during the early stages of star formation (Belloche et al. 2009). Laboratory and model efforts suggest that ice photochemistry on dust-grains during the protostellar stage produces complex molecules with high enough efficiency to explain the observed abundances (e.g. Muñoz Caro et al. 2002; Garrod & Herbst 2006; Garrod et al. 2008; Belloche et al. 2009, Chapter 10).

The ice-covered grains from the protostellar stage eventually become incorporated into the protoplanetary disk and there they collide and agglomerate to form larger and larger grains and eventually boulders and planetesimals. If the protostellar ices survive this stage, as suggested by models of Visser et al. (2009), the formed meteorites and comets may subsequently enrich planets with complex organic molecules. The importance of this last stage for the prebiotic chemistry on planets depends on the ice chemistry preceding planet formation. This chapter aims to quantify the formation of nitrogen-containing complex molecules in a large set of ice-mixtures of astrophysical interest and thus to deduce the necessary conditions to produce amino acids and other pre-biotically interesting molecules during star- and planet-formation.

Simple ices form in molecular clouds through hydrogenation and oxygenation of atoms and unsaturated molecules. Observations of ices before the onset of star formation reveal H₂O ice to be the main constituent, followed by CO and CO₂ (e.g. Whittet et al. 1998; Bergin et al. 2002). CH₄ and NH₃ ice probably form before the protostellar stage as well, but have only been detected around protostars (Gibb et al. 2004; Knez et al. 2005, Chapter 2). NH₃ is the main ice-carrier of nitrogen that is directly observed; N₂ may be present, but has no strong infrared transitions and CN-bearing species have an order of magnitude lower abundance (van Broekhuizen et al. 2005). NH₃ ice was first discovered by Lacy et al. (1998) and is now established to exist at abundances of 5–10% with respect to H₂O ice towards both high-mass and low-mass protostars (Gibb et al. 2004, Bottinelli et al. in preparation). From the NH₃ ice spectral profile and its proposed formation pathway through hydrogenation of nitrogen, NH₃ should form in the H₂O-rich ice layer. This ice phase also contains 20–30% CO₂ and ~5% CH₄. In contrast CH₃OH ice probably forms in a CO-rich ice layer frozen out on top of the H₂O-rich ice.

Organic nitrogen-containing molecules have been detected in the gas phase in the hot regions close to protostars, in galactic center clouds, in a low-mass outflow and in cometary outflows (see Herbst & van Dishoeck 2009 for review). The most abundant species are HCN, CH₃CN and HNCO, but the recently discovered C₃H₇CN and NH₂CH₂CN have been detected with relatively high fractional abundances with respect to H₂, 1.0×10^{-9} and 2.2×10^{-9} , respectively (Belloche et al. 2008, 2009).

The four nitrogen containing organic molecules searched for towards a sample of high-mass protostellar hot cores, HNCO, CH₃CN, C₂H₅CN and NH₂CHO, were all found

to have high rotational temperatures, while CHO-containing molecules without nitrogen could be divided into two temperature bins, tracing the hot core and the luke-warm envelope, respectively (Bisschop et al. 2007c). The high temperature of the nitrogen-bearing species is consistent with their formation and trapping in the bottom ice layer, the H₂O-rich ice phase, while CHO-containing species forming in the CO-rich outer ice layer are more exposed and thus desorb easier because of heat and non-thermal desorption pathways. The abundances of nitrogen-bearing complex molecules and of the other detected complex species are not correlated between sources, again consistent with the formation of nitrogen-containing and CHO-containing complex molecules in different phases of the ice; the CHO-containing complex species depend on the original CH₃OH content (Chapter 10), while the N-containing species do not.

Some complex nitrogen-bearing molecules have been detected in comets as well, including HNCO and CH₃CN (Altwegg et al. 1999; Crovisier et al. 2004b). The simplest amino acid, glycine, is yet undetected towards both comets and star-forming regions despite deep searches. The current abundance upper limits are $\sim 10^{-11}$ with respect to hydrogen in the Orion star forming region, and 1×10^{-10} in the cold envelope and 7×10^{-9} in the hot core of the solar-type protostar IRAS 16293-2422 (Combes et al. 1996; Ceccarelli et al. 2000). Amino acids are however found in meteorites where more sensitive analysis methods are available (Engel & Macko 1997) – these acids probably formed during the proposed aqueous phase of the meteorite.

The photochemistry of NH₃ containing ices was first investigated for astrophysically relevant ice mixtures by Hagen et al. (1979), who irradiated a CO:H₂O:NH₃:CO₂ 50:1:1:0.09 ice at ~ 10 K with a UV lamp peaking at 160 nm. HNCO, H₂CO, NH₂CHO and HCOOH were identified among the products and unidentified larger molecules with molecular masses up to 514 amu were recorded mass-spectrometrically following warm-up of the photolyzed ice residue to room temperature. There is thus qualitative evidence for a nitrogen-based complex chemistry upon irradiation of NH₃-containing ice mixtures. Other early experimental studies investigated the qualitative effects of varying different species to the mixtures and changing the original abundance ratios (e.g. Allamandola et al. 1988; Grim et al. 1989; Schutte et al. 1993). Two of the main results were the relative ease at which XCN compounds, especially OCN⁻, and NH₂-containing molecules form in NH₃-containing ices. The largest infrared detected molecule is C₆H₁₂N₄ (Bernstein et al. 1995; Muñoz Caro & Schutte 2003).

Bernstein et al. (2002) and Muñoz Caro et al. (2002) first reported on efficient amino acid production following irradiation of ices in similar high-vacuum experiments; the amino acids were detected using gas chromatography and mass spectrometry of the irradiated ice residue after the sample was heated to room temperature. These studies were followed up with both models and isotopically labeled experiments to constrain the formation mechanisms (Woon 2002; Muñoz Caro et al. 2004; Elsila et al. 2007; Nuevo et al. 2007; Lee et al. 2009). The general conclusion was that amino acids form through a variety of radical-radical reactions; amino acid formation is more efficient in HCN-containing matrices, but pathways from NH₃ exist as well. It is however still unclear when these amino acids form, i.e. if there is a cold formation pathway during UV irradiation of the ice or if heating to room temperature is required.

Overall these experimental results are enticing since they suggest that amino acid production may be possible in interstellar ices. Final yields in a laboratory setting provide little information on the final fraction under different astrophysical conditions, however – the reported carbon-conversion efficiencies, up to 0.5%, may be a result of the experimental technique. These experiments were all carried out under high-vacuum conditions, where thick ices (tens of μm) were deposited at ~ 10 K while irradiating the ice to produce the maximum amount of radicals. The photolyzed ices were then heated to room temperature and the residue analyzed mass-spectrometrically. This procedure was necessary when carrying out experiments under high-vacuum and employing transmission spectroscopy. It is however difficult to deduce from these experiments which molecules form under interstellar conditions and at what abundances. Specifically, none of these studies provide any quantitative data on reaction rates of nitrogen-containing molecules. They thus do not present data that can be included in astrochemical models to test whether ice photochemistry produces the correct amounts and correct abundance ratios of complex molecules, under interstellar conditions and timescales, compared to astrophysical observations.

Despite a lack of this kind of data, a complex nitrogen chemistry was incorporated in a recent grain-gas model of the complex ice chemistry in protostellar envelopes and the subsequent desorption in the hot core close to the protostar (Garrod et al. 2008). The model assumes a perfectly mixed ice, which probably explains why it over-produces NH₂CHO, but under-produces CH₃CN and CH₃NH₂; if NH₃ is mainly formed in the H₂O-rich layer it will have more access to CH₄-dissociation products than to CO-reaction products. Model improvements are mainly limited by the lack of quantitative data on the NH₃ ice photochemistry.

Such quantitative data should be possible to derive from simpler binary ice mixtures, since e.g. the CH₃ diffusion barrier in all H₂O dominated ices should be approximately the same. Reaction barriers only depend on the two radicals reacting and while effective photodissociation cross sections may change with temperature or ice mixture because of changing diffusion barriers (Chapter 10), the branching ratio should solely depend on the UV lamp spectrum. Quantifying the complex ice chemistry of astrophysically relevant ice mixtures should thus be possible by first extracting physical quantities from simple, well-constrained ice mixtures and then performing experiments on more complicated mixtures to ensure that these results are consistent with predictions from the simpler ice experiments.

This chapter presents the production of moderately complex species, up to glycine, in a large set of ice mixtures during irradiation at 20 K and during warm-up between 20 and 230 K. In contrast to most previous experiments the irradiation is done after deposition and the complex molecule formation is followed *in situ* using infrared spectroscopy and temperature programmed desorption (TPD). The main part of the chapter focuses on the photodesorption, photodissociation and product formation during irradiation of pure and binary ices. Section 11.4 then presents the quantification of the same products in more complicated mixtures together with TPD experiments to identify the most complex photoproducts accessible for *in situ* study. The TPD experiments are performed following irradiation of an astrophysical ice analogue and five other mixtures, which are used to constrain the nature of the desorbing species. The results are used in the Discussion

section to constrain photodissociation branching ratios, relative diffusion barriers and the reaction pathways that the observed molecules form through. The implications for understanding ice chemistry in astrophysical environments are discussed, followed by proposed new experiments to further constrain the chemistry.

11.2 Experimental

All experiments are carried out on the set-up CRYOPAD under ultra-high vacuum conditions ($\sim 10^{-9}$ – 10^{-10} mbar). Pure and mixed ices are deposited diffusively at 18 K by introducing a gas (mixture) in the vacuum chamber along the surface normal of a gold substrate, which is temperature controlled down to 18 K with a 2 K uncertainty. The gas mixtures are prepared in a separate glass manifold with a base pressure of 10^{-4} mbar to have a total pressure of 10–20 mbar. The CO_2 , NH_3 and CH_4 gases have a minimum purity of 99.9% (Indugas). Samples containing H_2O are prepared from the vapor pressure of de-ionized H_2O , further purified through several freeze-thaw cycles.

The ices are probed through infrared spectroscopy in reflection-absorption mode (RAIRS) and the desorbed molecules during warm-up are investigated with a quadrupole mass spectrometer (QMS), facing the substrate. As described in Chapters 8–10 relative RAIRS band strengths are consistent with relative transmission band strengths and thus certain within 20–30%. Absolute band strengths have a 50% uncertainty, but this only affects the derived photodesorption rates – not the quantification of the chemistry.

The original ice mixture as well as changes in the ice composition induced by UV irradiation are quantified using RAIRS, while the QMS is employed to secure band identifications of photoproducts. The UV irradiation is provided by a hydrogen-discharge lamp with UV emission around Ly- α and through a broader continuum between 6 and 11.5 eV (Muñoz Caro & Schutte 2003). All ices are irradiated with a UV flux of $1.1(\pm 0.4) \times 10^{13} \text{ s}^{-1} \text{ cm}^{-2}$ except for an experiment aimed to determine the photodesorption yield (Exp. 1), where a four times higher flux is used.

Table 11.1 lists the photochemistry experiments in terms of their mixture composition and total thickness. The set of experiments has been designed to test the influence of different combinations of H_2O , CO_2 , NH_3 and CH_4 on the complex product formation. Experiment 18 was chosen to mimic the H_2O -rich phase observed towards low-mass protostars (Chapter 2). All experiments are UV irradiated at 20 K followed by warm-up by 1 K min^{-1} to 150–230 K, while acquiring RAIRS every 10 min and monitoring the desorption products with the QMS at a range of mass signals between 2 and 62 amu. The ice thicknesses range between ~ 8 –78 monolayers (ML). This ice thickness regime is similar to what is expected in the dense and cold stages of star formation. Each ice in experiment 2–18 was irradiated for 6 hours, resulting in a UV fluence of $\sim 2.3 \times 10^{17} \text{ cm}^{-2}$. This is comparable to the fluence an ice in a cloud core is exposed to during 10^6 years because of cosmic-ray induced UV photons at a flux of 10^4 cm^{-2} (Shen et al. 2004).

Table 11.1. The composition and thickness of all photochemistry experiments.

Exp.	H ₂ O	CO ₂	CH ₄	NH ₃	Thickness (ML)	$\phi^a(10^{-18}\text{cm}^2)$
1				1	8	
2				1	51	1.5±0.5
3	1				43	
4		1			15	
5			1		47	
6	1			1	54	1.7±0.6
7	4			1	43	5.6±2.0
8		1		2.5	44	5.7±2.0
9			3	2	45	2.2±0.8
10	1	1.5			21	
11	6	1			35	
12	1		3		42	
13	2		1		37	
14		1	2		33	
15	1	1		1	69	
16	1		1	1	66	
17		1	1	1	78	
18	100	20	8	12	66	

^aThe initial NH₃ photodestruction cross section

11.3 Photochemistry in pure ices and binary ice mixtures

When quantifying the chemistry in pure ices and binary ice mixtures, the initial ice compositions, and the photodesorption and photodissociation yields are calculated from the listed ice bands in Table 11.2. Table 11.2 also lists the photoproducts considered in this section, together with the infrared bands used for quantification, transmission band strengths and literature references on the ice spectra. Most photoproduct bands are easily identified from their spectral positions alone, but a few bands require further analysis to assign them to specific complex species. The TPD experiments mentioned in this section are discussed in detail §11.4.2

Each abundance is quantified by fitting a local baseline around the spectral feature and then fitting one or multiple Gaussians to the band of interest using a personal IDL routine. The automatic fits are visually inspected to ensure that the fitted Gaussians are consistent with bands in pure and ice mixture reference spectra.

11.3 PHOTOCHEMISTRY IN PURE ICES AND BINARY ICE MIXTURES

Table 11.2 – The original ice infrared bands and the photoproduct spectral features used for quantification.

Species	Band (cm ⁻¹)	Band strength ^a (cm ⁻¹)	Reference
CH ₄	1300	6.1×10 ⁻¹⁸	Moore & Hudson (1998)
NH ₃	1070	1.7×10 ⁻¹⁷	D'Hendecourt & Allamandola (1986)
CO ₂	2343	7.6×10 ⁻¹⁷	Gerakines et al. (1995)
H ₂ O	1670	1.2×10 ⁻¹⁷	Gerakines et al. (1995)
C ₂ H ₆	2976	1.1×10 ⁻¹⁷	Moore & Hudson (1998) ^b
	821	1.9×10 ⁻¹⁸	Pearl et al. (1991)
C ₂ H ₄	1436	2.9×10 ⁻¹⁸	Moore & Hudson (1998) ^b
N ₂ H ₄	2768	~1.5×10 ⁻¹⁷	assumed from NH ₃
CH ₃ NH ₂	2794	~5×10 ⁻¹⁸	assumed from C ₂ H ₆
HCN	2087	5.1×10 ⁻¹⁸	Gerakines et al. (2004)
H ₂ CO	1500	3.9×10 ⁻¹⁸	Schutte et al. (1993)
CH ₃ OH	1026	2.8×10 ⁻¹⁷	D'Hendecourt & Allamandola (1986)
CH ₃ CH ₂ OH	1044	7.3×10 ⁻¹⁸	Moore & Hudson (1998) ^b
CH ₃ CHO	1350	6.1×10 ⁻¹⁸	Moore & Hudson (1998) ^b
CO	2139	1.1×10 ⁻¹⁷	Gerakines et al. (1995)
CO ₃	2045	~7.6×10 ⁻¹⁷	assumed from CO ₂
O ₃	1045	1.4×10 ⁻¹⁷	Brewer & Wang (1972)
OCN ⁻	2165	1.3×10 ⁻¹⁶	van Broekhuizen et al. (2005)

^a The uncertainties in the tabulated transmission band strengths is ~20–30% when comparing results from different references, ice mixtures and ice temperatures.

^b In a H₂O ice matrix.

11.3.1 CH₄, NH₃ and CH₄:NH₃ ice photolysis

Figure 11.1 shows the spectra before and after photolysis of pure CH₄ ice, pure NH₃ ice and a CH₄:NH₃ ~3:2 ice mixture, all at 20 K. The bands used to quantify the considered photoproducts, C₂H₆, C₂H₄, N₂H₄, CH₃NH₂ and HCN, are marked. The strong C₂H₆ bands are assigned from spectral comparison alone, since these bands have no spectral overlap with other possible product bands (Moore & Hudson 1998). The C₂H₄ band at 1436 cm⁻¹ is weaker and partly overlapping with other bands, and its disappearance together with the C₂H₆ around 60 K was used to confirm the C₂H₄ assignment. The same assignments were made by Gerakines et al. (1996) and Moore & Hudson (1998).

The observed broad band at 2794 cm⁻¹ in the pure NH₃ ice agrees in band position and width with one of the N₂H₄ ice bands reported by Roux & Wood (1983). The N₂H₄ assignment is, however, tentative since no desorption data exist on N₂H₄ and most other N₂H₄ features overlap with strong NH₃ bands. The other likely pure NH₃ photoproduct, N₂H₂, is excluded as a carrier from comparison with spectra by Blau et al. (1961). Two other bands form in the pure NH₃ ice upon UV irradiation, at 2111 and 1507 cm⁻¹. The 2111 cm⁻¹ is probably due to N₂H₄ as well, while the 1507 cm⁻¹ band can be assigned to NH₂ (Gerakines et al. 1996) though NH_{3/4}⁺ are candidates as well (Thompson & Jacox 2001). During warm-up most of the band disappears before NH₃ desorption, consistent with NH₂ as a main carrier, but with an unconfirmed assignment, its formation cannot be

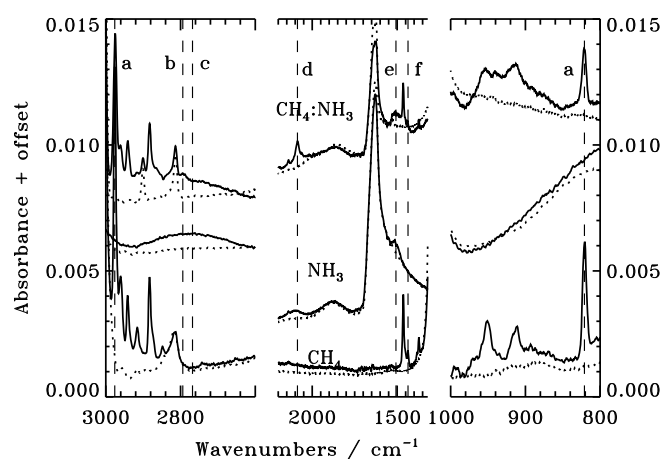


Figure 11.1 – The initial spectra (dotted lines) and spectra after photolysis (solid lines) of pure CH₄ ice, pure NH₃ ice and a CH₄:NH₃: ~3:2 mixture, all at 20 K. The bands used for quantifying the a) C₂H₆, b) CH₃NH₂, c) N₂H₄, d) HCN, e) NH₂ and f) C₂H₄ ice abundances are marked with dashed lines.

quantified.

The HCN and CH₃NH₂ ice features in the photolyzed CH₄:NH₃ ice mixture spectrum are assigned by comparing laboratory ice spectra from the NASA Goddard ice database by Moore et al. (<http://www-691.gsfc.nasa.gov/cosmic.ice.lab/spectra.html>) with spectra from the photolyzed CH₄:NH₃ ice mixture during warm-up. During the TPD experiments following photolysis, mass patterns consistent with HCN and CH₃NH₂ desorption are visible at 110 and at 120 K. Figure 11.2 shows the difference RAIR spectrum of the photolyzed CH₄:NH₃ ice mixture between 120 and 100 K, i.e. the spectrum acquired at 100 K subtracted from the spectrum acquired at 120 K. This reveals the spectral features of species that desorb in this temperature interval and is thus provides a method for band identifications. The agreement of this difference spectrum with the HCN + CH₃NH₂ bands is excellent. Figure 11.2 also shows that the bands selected to quantify HCN and CH₃NH₂ are distinguishable at 20 K.

Quantifying the formation of ice species with respect to the initial ice composition requires known transmission band strengths – all spectra here are acquired with RAIRS, but the relative band strengths are the same in transmission and reflection-absorption mode as long as the bands are not too strong. Transmission band strengths are available for C₂H₆, C₂H₄ and HCN ice, but not for N₂H₂ or CH₃NH₂ ice. The latter two band strengths are estimated by assuming a similar N-H/C-H band strength in the more complex molecules as in NH₃ and C₂H₆.

Figure 11.3 shows the formation of C₂H₆, C₂H₄, N₂H₂, HCN and CH₃NH₂ as a function of UV fluence in pure CH₄ ice, in pure NH₃ ice and in the CH₄:NH₃ ~ 3:2 ice mixture. The C₂H₆ and N₂H₄ production are only reduced by ~40% each in the mixture

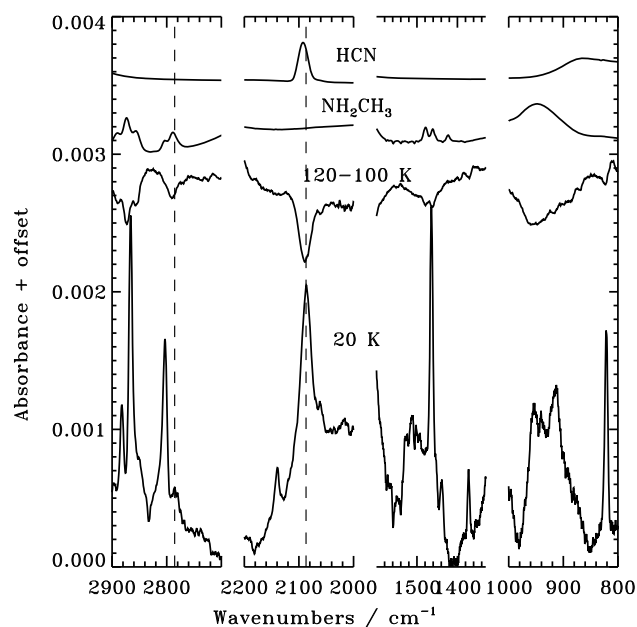


Figure 11.2 – Starting from the bottom the figure shows a photolyzed CH_4NH_3 ice spectrum at 20 K, a difference spectrum during warm-up of the same ice mixture, a CH_3NH_2 spectrum (mixed with H_2O) and a pure HCN ice spectrum. In the difference spectrum negative peaks signify desorption of the band carrier. The dashed lines show the agreement between the reference spectra and the photolysis experiment for the HCN and NH_2CH_3 bands used for quantification.

and this is with respect to the total ice thickness. Their production rates are thus the same, within the uncertainties, in the pure CH_4 ice and in the ice mixture with respect to the CH_4 and NH_3 abundances. The abundant C_2H_6 formation in the ice mixture indicates that it is mainly the formation of larger hydrocarbons that is suppressed in favor of HCN and CH_3NH_2 production in the ice mixture. This is consistent with the reduction in C_2H_4 production, which is evidence of that CH_2 , an ingredient in both C_2H_4 and C_3H_8 formation, is quickly consumed by reactions with NH_x in the ice mixture.

The two molecules forming from reactions of NH_3 and CH_4 fragments, CH_3NH_2 and HCN, depend differently on UV fluence (Fig. 11.3d.). The CH_3NH_2 ice abundance reaches steady-state faster than any other investigated molecule does, while the formation rate of HCN increases with fluence, indicative of a HCN formation pathway from first-generation photoproducts, such as CH_3NH_2 and CH_2NH .

By comparing the initial C_2H_6 formation in Fig. 11.3a and C_2H_4 formation in 11.3b, it is possible to constrain the CH_4 photodissociation branching ratio. This is done below using the initial formation cross sections of C_2H_6 and C_2H_4 in the pure CH_4 ice, which are $(3.2 \pm 1.3) \times 10^{-19}$ and $(3.6 \pm 1.5) \times 10^{-20} \text{ cm}^2$ after $4 \times 10^{16} \text{ photons cm}^{-2}$. Gerakines

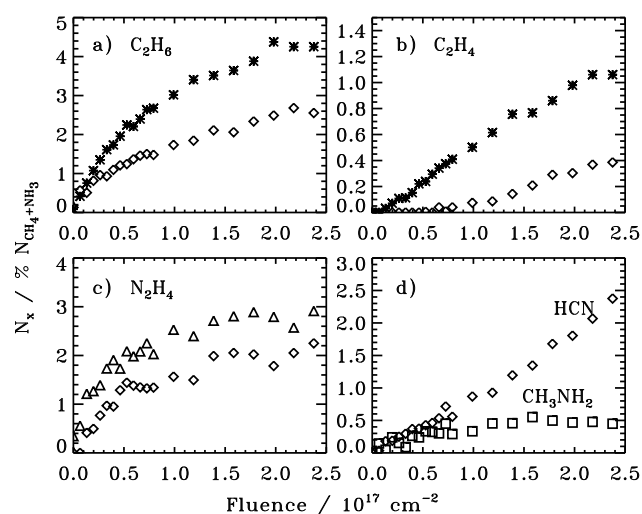


Figure 11.3 – The relative formation of five complex molecules, with respect to the initial total ice abundance, in pure CH₄ ice (stars), in pure NH₃ ice (triangles) and in a CH₄:NH₃ ~ 3:2 ice mixture (diamonds and squares) as a function of UV fluence at 20 K.

et al. (1996) finds a comparable C₂H₆/C₂H₄ product ratio (8/1) following pure CH₄ ice photolysis.

The chemistry in the pure and mixed ices are then proposed to proceed as shown in Fig. 11.4, where the reaction scheme for the mixed ice is constructed by combining the CH₄ and NH₃ reaction schemes with the bridging HCN and CH₃NH₂ reactions. The reaction schemes clearly show the additional number of steps required to form HCN compared to CH₃NH₂, which explains the initial delay in the HCN production. The early steady-state of CH₃NH₂ suggests that it easily photodissociates into HCN, even though the process probably requires several steps, and that this is an important formation path to HCN in the ice. This is also consistent with the almost constant formation rate of HCN once the initial delay is overcome.

11.3.2 CH₄:H₂O ice mixture photolysis

Figure 11.5 shows the initial and photolyzed spectra of pure CH₄ ice and a CH₄:H₂O ~ 3:1 mixture, both at 20 K. There are no identified photoproducts following pure H₂O ice photolysis (not shown). This is in contrast with e.g. Gerakines et al. (1996), who detected OH and H₂O₂ formation. The observed rates were low, however, and neither would be expected to be observable at the ice thicknesses and UV fluences employed in this study. The photolyzed CH₄ and CH₄:H₂O ice spectra are plotted together with pure CH₃OH, H₂O, CH₃CH₂OH and CH₃CHO ice spectra to justify the complex photoproduct assignments. The most isolated bands of each complex ice species are used for quantification.

11.3 PHOTOCHEMISTRY IN PURE ICES AND BINARY ICE MIXTURES

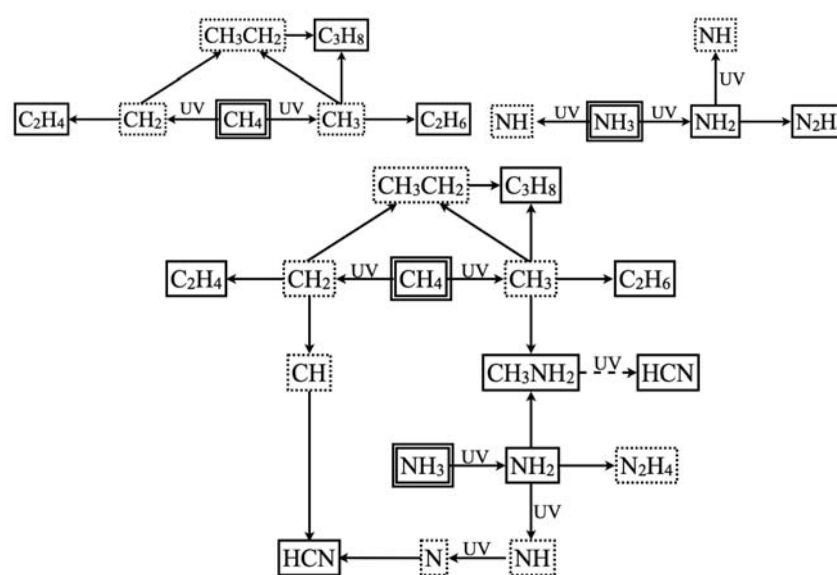


Figure 11.4 – The proposed reactions schemes following UV photolysis of pure CH_4 ice (upper left), pure NH_3 ice (upper right) and a $\text{CH}_4:\text{NH}_3$ ice mixture (bottom scheme). Solid boxes mark detected species and dotted boxes undetected ones. Dashed arrows mark photodissociation through several steps.

Similarly to the $\text{CH}_4:\text{NH}_3$ photochemistry, the formation rate of C_2H_6 does not change significantly between the pure CH_4 ice and the $\text{CH}_4:\text{H}_2\text{O}$ 3:1 mixture, while the C_2H_4 production is significantly lowered in the latter case. Of the new complex molecules in the $\text{CH}_4:\text{H}_2\text{O}$ mixture, CH_3OH forms the fastest, but reaches a similar steady-state level to $\text{CH}_3\text{CH}_2\text{OH}$. H_2CO , CH_3CHO and $\text{CH}_3\text{CH}_2\text{OH}$ all start to form after a certain fluence level is reached, indicative of a second or later generation of photoproducts. CH_3CHO forms last. Qualitatively the product assignments agree with Moore & Hudson (1998) who also found a comparable $\text{CH}_3\text{OH}/\text{CH}_3\text{CH}_2\text{OH}$ product ratio in their $\text{CH}_4:\text{H}_2\text{O}$ 1:2 ice mixture.

$\text{CH}_3\text{CH}_2\text{OH}$ and CH_3CHO are also photoproducts of pure CH_3OH ice (Chapter 10) and their product ratio is consistent between the CH_3OH and the $\text{CH}_4:\text{H}_2\text{O}$ photolysis experiments. The formation path for $\text{CH}_3\text{CH}_2\text{OH}$ must however be different in the two experiments since the $\text{CH}_3\text{CH}_2\text{OH}$ to CH_3OH ratio is one order of magnitude higher in the $\text{CH}_4:\text{H}_2\text{O}$ ice than in the CH_3OH ice following irradiation with the same fluence. Figure 11.7 shows that $\text{CH}_3\text{CH}_2\text{OH}$ probably forms from $\text{C}_2\text{H}_5 + \text{OH}$ in the $\text{CH}_4:\text{H}_2\text{O}$ mixture versus $\text{CH}_3 + \text{CH}_2\text{OH}$ in the CH_3OH ice (Chapter 10), while CH_3CHO is proposed to form through photodissociation of $\text{CH}_3\text{CH}_2\text{OH}$ or radical-radical reactions between CH_3 and HCO in both cases; both formation paths are consistent with the late onset of CH_3CHO formation. The delay in H_2CO and $\text{CH}_3\text{CH}_2\text{OH}$ formation is also explained

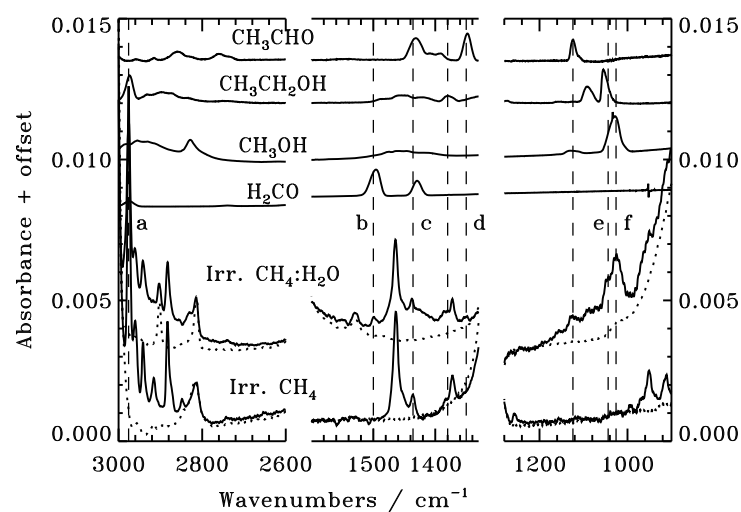


Figure 11.5 – The initial spectra (dotted lines) and spectra after photolysis (solid lines) of pure CH₄ ice and a CH₄:H₂O~3:1 mixture, both at 20 K. The bands used for quantifying the a) C₂H₆, b) H₂CO, c) C₂H₄, d) CH₃CHO, e) CH₃CH₂OH and f) CH₃OH ice abundances are marked with dashed lines.

by the reaction scheme, which shows that both species require one more reaction step compared to CH₃OH and C₂H₆ formation.

11.3.3 Pure CO₂ and CH₄:CO₂ ice photolysis

Pure CO₂ ice photolysis results in CO, CO₃ and O₃ formation, consistent with Gerakines et al. (1996). Figure 11.8 shows that in the CH₄:CO₂ ice mixture CO and CO₃ still form and so do C₂H₆ and C₂H₄. In addition, features belonging to CH₃OH, H₂CO and CH₃CHO are identified. HCOOH probably forms as well, but its most distinct band overlaps with features from H₂CO, CH₃CHO and CH₃COOH. The contribution of HCOOH to the 1700 cm⁻¹ complex can be investigated through difference spectra during warm-up, since the HCOOH desorption temperature is known from Chapter 10. This is shown in Fig. 11.9, where a HCO-X band disappears in the 130–160 K temperature range, where HCOOH desorbs. It is however not possible to determine the HCOOH formation during irradiation.

Therefore the quantitative analysis focuses on the other, securely identified ice photo-products. CO₃ and O₃ formation changes most dramatically between pure CO₂ photolysis and CH₄:CO₂ photolysis; the formation rates decrease with an order of magnitude in the mixture (Fig. 11.10). The CO formation rate does not change significantly indicating that CO is relatively unreactive. The extremely low CO₃ production in this ice mixture can be explained by fast hydrogenation of CO₃ to form H₂CO₃. Moore (1991) detected abundant H₂CO₃ during warm-up of an irradiated H₂O:CO₂ ice mixture and similar bands are also

11.3 PHOTOCHEMISTRY IN PURE ICES AND BINARY ICE MIXTURES

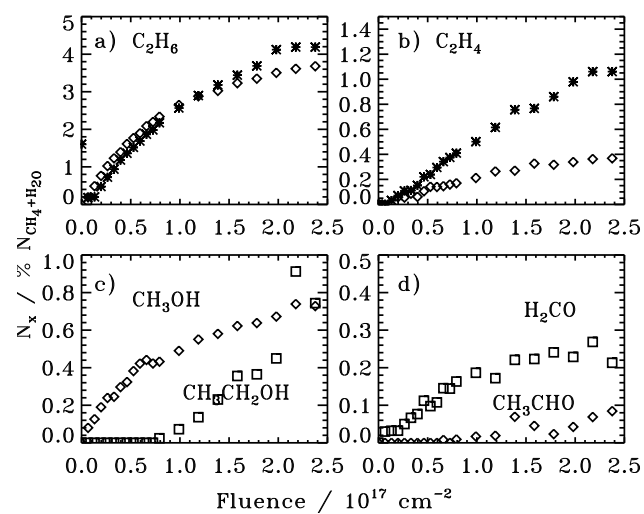


Figure 11.6 – The relative formation of six complex molecules, with respect to the initial total ice abundance, in pure CH_4 ice (stars) and in a $\text{CH}_4:\text{H}_2\text{O}\sim 3:1$ ice mixture (diamonds and squares) as a function of UV fluence at 20 K.

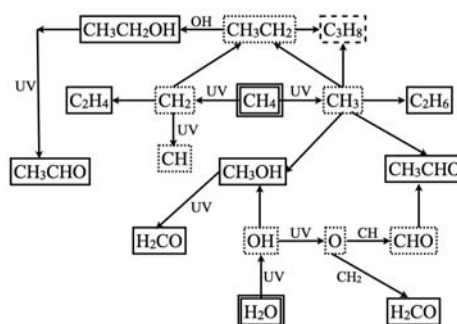


Figure 11.7 – The proposed reactions scheme following UV photolysis of a $\text{CH}_4:\text{H}_2\text{O}$ ice mixture. Solid boxes mark detected species, dashed boxes represent tentatively detected species from RAIRS or TPD curves and dotted boxes undetected species.

present during warm-up of the $\text{CH}_4:\text{CO}_2$ ices to 200 K.

Of the three new complex species, CH_3OH is formed at a similar rate compared to in the $\text{CH}_4:\text{H}_2\text{O}$ mixture, while CH_3CHO and H_2CO form at a higher rate. CH_3OH can form either through hydrogenation of CO or CH_3+OH reactions – its early steady-state suggests that CH_3+OH is the main formation path, since the CO continues to increase throughout the experiment and so should CH_3OH if it formed from CO.

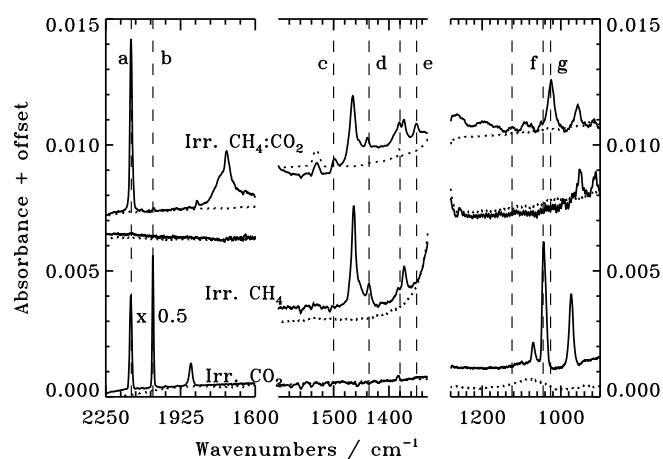


Figure 11.8 – The initial spectra (dotted lines) and spectra after UV photolysis (solid lines) of pure CO₂ ice, pure CH₄ ice and a CO₂:CH₄ ~1:2 mixture, all at 20 K. The bands used for quantifying the a) CO, b) CO₃, c) H₂CO, d) C₂H₄, e) CH₃CHO, f) O₃ and g) CH₃OH ice abundances are marked with dashed lines.

Figure 11.11 shows these reaction paths and proposed reaction paths for all infrared-detected products. The faster onset of CH₃CHO production in the CH₄:CO₂ ice mixture compared to the CH₄:H₂O ice mixture suggests that CH₃ + HCO is the dominating formation path in the CH₄:CO₂ ice rather than CH₃CH₂OH photodissociation. HCOOH formation may occur through two different reaction pathways: hydrogenation of CO₂ and CO+HCO reactions. The former is prohibitively slow for thermalized hydrogen atoms (Bisschop et al. 2007b), but it may still be fast for energetic species. In either case, the experiments here show that any kind of hydrogenation of CO and CO₂ is definitely less efficient than hydrogenation of the radical CO₃. This is in agreement with previous comparison of molecule and atom hydrogenation efficiencies (Hiraoka et al. 1998).

11.3.4 CO₂:NH₃ ice mixture photolysis

Irradiation of a CO₂:NH₃ ice mixture produces a complex ice spectrum (Fig. 11.12). This has been previously observed for ice mixtures containing NH₃, H₂O and CO and many of the new broad features can be ascribed to NH₄⁺:XCOO⁻ salts (Muñoz Caro & Schutte 2003). NH₂CHO has several spectral features in the 1400-1700 cm⁻¹ region and probably contributes as well. Because of the overlap between different bands shown in Fig. 11.12, only the formation of CO and OCN⁻ (from its 2161 cm⁻¹ band) can be quantified at this stage.

OCN⁻ is a common product from UV processing of C, O and NH₃ containing ices and its formation in the CO₂:NH₃ ice mixture is consistent with previous studies (e.g. van Broekhuizen et al. 2004). Figure 11.13 shows that similarly to what was observed

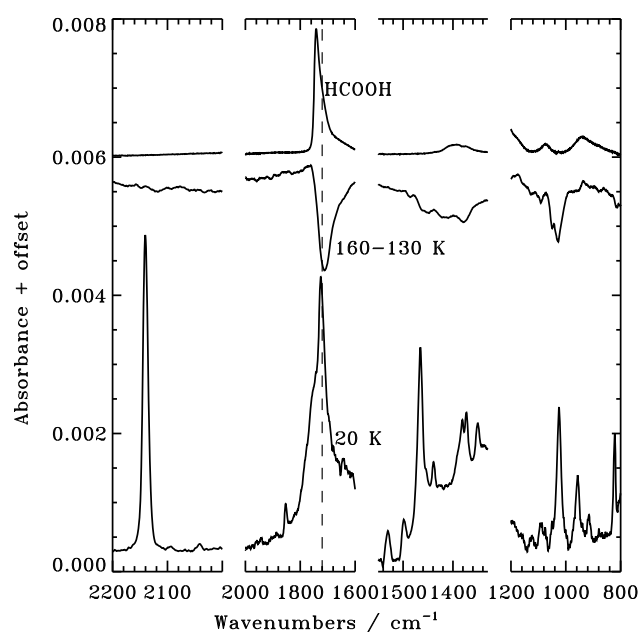


Figure 11.9 – Starting from the bottom the figure shows a photolyzed $\text{CO}_2:\text{CH}_4$ ice spectrum at 20 K, a difference spectrum during warm-up of the same ice mixture, and a pure HCOOH spectrum. In the difference spectrum negative peaks signify desorption of the band carrier.

for HCN in the $\text{CH}_4:\text{NH}_3$ mixture, OCN^- is not produced immediately at the onset of irradiation (i.e. within 10 minutes), indicative of a multi-step formation process. This explains the low yield of OCN^- with respect to NH_4^+ ; the lower limit on NH_4^+ formation is more than an order of magnitude greater than the OCN^- production. OCN^- is thus not the main counter ion of NH_4^+ . Figure 11.13 also shows that OCN^- does not desorb below 170 K.

With only two band assignments, the $\text{CO}_2:\text{NH}_3$ reaction scheme is speculative. The pathway to HNC and further to OCN^- may either be through $\text{CO}+\text{NH}$ or $\text{CO}+\text{NH}_2$ followed by photodissociation. From the $\text{H}_2\text{O}:\text{CO}_2$ and $\text{CH}_4:\text{CO}_2$ ice mixtures, both H_2CO_3 and HCOOH are expected products in the $\text{CO}_2:\text{NH}_3$ ice photolysis experiment. These two acids may very well be the main counter ions to NH_4^+ , since in the presence of NH_3 they should both be converted into their salt counterparts HCO_3^- and HCOO^- (Schutte & Khanna 2003).

11.3.5 The effect of H_2O at different concentrations

Figure 11.14 shows the spectra of pure NH_3 , $\text{H}_2\text{O}:\text{NH}_3$ 1:1 and $\text{H}_2\text{O}:\text{NH}_3$ 4:1 ice mixtures before and after the ices are irradiated with a UV fluence of $2.3 \times 10^{17} \text{ cm}^{-2}$. Adding different amounts of H_2O to NH_3 ice suppresses the production of the 2111 cm^{-1} and 2768 cm^{-1} features, observed in the pure ice photolysis experiment and there ascribed to N_2H_4 ; neither is observed in any of the $\text{H}_2\text{O}:\text{NH}_3$ ice mixture experiments, though

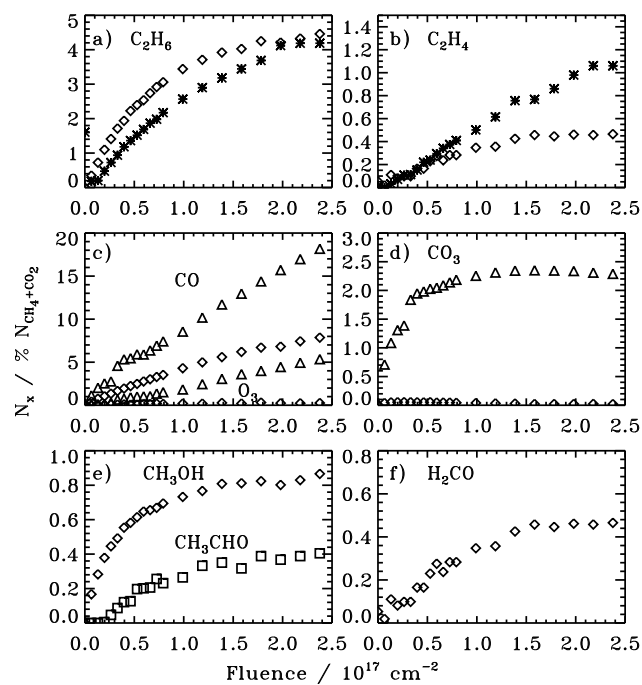


Figure 11.10 – The relative formation of eight photoproducts, with respect to the initial total ice abundance, in pure CH₄ ice (stars), pure CO₂ ice (triangles) and a CH₄:CO₂ ~ 2:1 ice mixture (diamonds and squares) as a function of UV fluence at 20 K.

overlap between the 2768 cm⁻¹ band and the H₂O feature wing prevents a strict upper limit. The 1507 cm⁻¹ band is still present in the H₂O mixtures. In addition, at least one new feature appears in the 4:1 ice mixture, and probably in the 1:1 ice as well, at 1470 cm⁻¹. In general the combined band around 1500 cm⁻¹ is more pronounced the more H₂O is added, indicative of either the onset of an acid-base chemistry or efficient trapping of NH₂; additional irradiation experiments are required to distinguish between the two carrier scenarios. Without a more strict assignment, the chemistry cannot be further quantified in the H₂O:NH₃ mixtures.

Photolysis of the H₂O:CO₂ mixtures results in several broad features, which are due to a combination of HCOOH and H₂CO₃. The bands cannot be easily separated during irradiation and therefore this chemistry is equally difficult to quantify as the H₂O:NH₃ chemistry.

In the CH₄:H₂O 3:1 and 1:2 ice mixtures C₂H₆, CH₃OH, CH₃CHO, CH₃CH₂OH and H₂CO all clearly form upon UV irradiation. The formation of the first four complex species is quantified in Fig. 11.15 with respect to the initial CH₄ ice abundance. Increasing the H₂O concentration reduces the relative C₂H₆ formation and increases the relative

11.3 PHOTOCHEMISTRY IN PURE ICES AND BINARY ICE MIXTURES

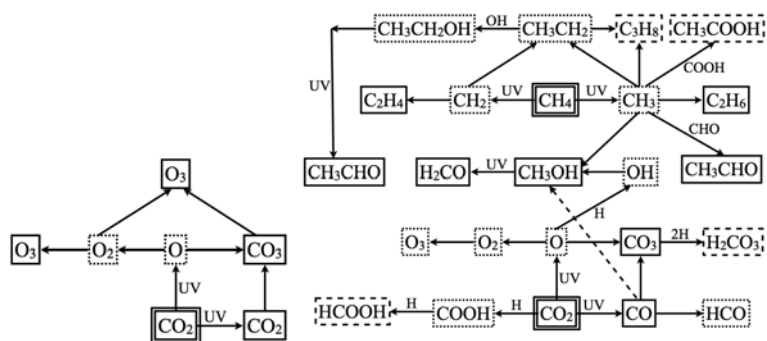


Figure 11.11 – The proposed reactions schemes following UV photolysis of pure CO_2 ice (left-hand scheme) and a CH_4 : CO_2 ice mixture (right-hand scheme). Solid boxes mark detected species, dashed boxes tentatively detected species and dotted boxes represent undetected ones. Dashed arrows mark formation pathways that require several steps.

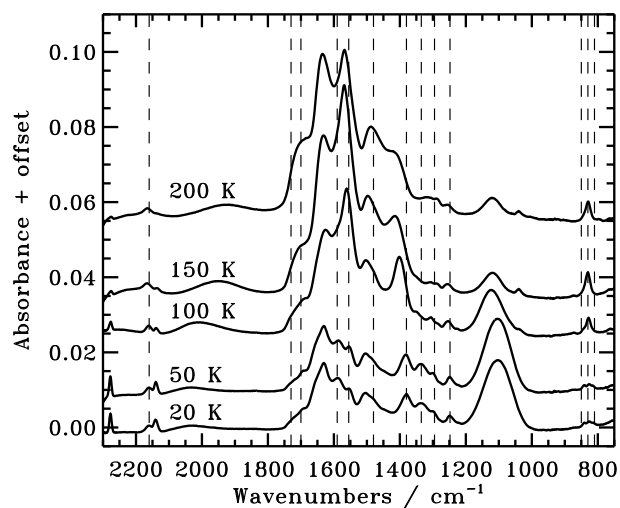


Figure 11.12 – Spectrum of irradiated NH_3 : CO_2 ice during warm-up. All features exclusive to photolysis of CO_2 : NH_3 ice mixtures compared to pure ices are marked with dashed lines. The OCN^- feature is at 2161 cm^{-1} .

formation rates of CH_3OH , CH_3CHO and H_2CO as expected when increasing the relative OH/CH_3 radical ratio in the ice.

During irradiation there is no obvious evidence for a slower radical diffusion because of higher binding energies in a H_2O -rich ice. During warm-up there are some differences between the two ice mixtures, however (Fig. 11.16). The CH_3OH and CH_3CHO abundances increase in both mixtures with temperature, but the CH_3CHO abundance increases more in H_2O -rich ice and the CH_3OH abundance in the H_2O -poor ice, indicative of different diffusion conditions in the H_2O -poor and the more strongly bound H_2O -rich

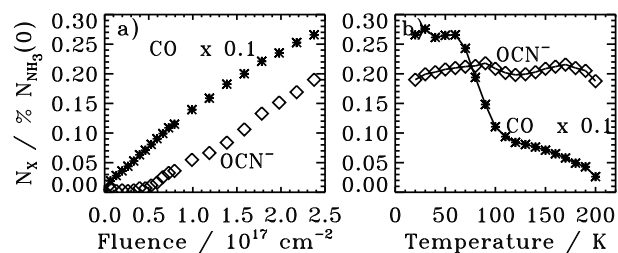


Figure 11.13 – The evolution of the OCN⁻ and CO abundances as a function of UV fluence at 20 K, and as a function of temperature during warm-up.

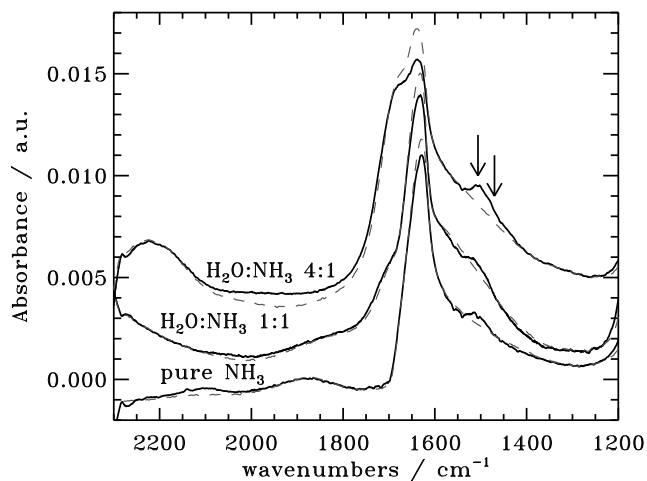


Figure 11.14 – Spectra of pure NH₃ ice, NH₃:H₂O 1:1 and 1:4 ice mixtures, before irradiation at 20 K (dashed lines) and after UV irradiation at 20 K (solid lines). The 1507 and 1470 cm⁻¹ features are marked with arrows.

mixture.

11.3.6 NH₃ ice photodesorption

The efficiency of photochemistry in both pure ices and mixtures is limited by the formation rates of radicals through photodissociation, which is discussed in the next subsection, and by the photodesorption rate, which continuously desorbs ice. Figure 11.17 shows the loss of NH₃ ice at 20 K as a function of UV fluence due to a combination of bulk dissociation and surface photodesorption, calculated from the 1070 cm⁻¹ band. The photodesorption yield is determined from the linear decrease in ice thickness, visible at later times, while the bulk dissociation follows an exponential decay (Öberg et al. 2009b,a). The combined linear and exponential fits result in a NH₃ photodesorption yield of $(1.2 \pm 0.7) \times 10^{-3}$ per incident UV photon. The main error comes from the ice thickness uncertainty; the fit error is ~15%.

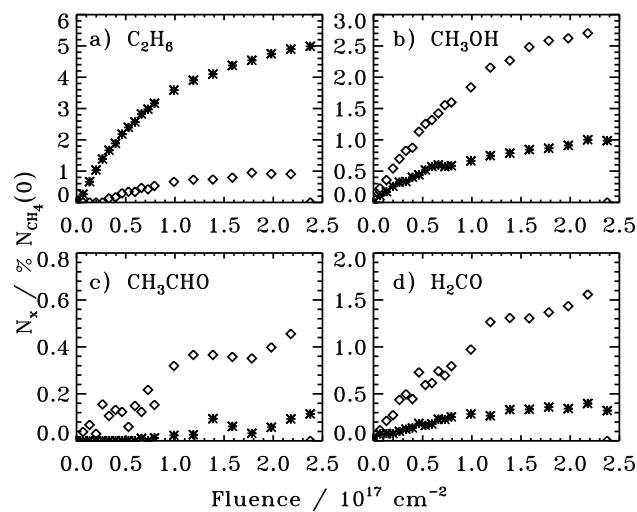


Figure 11.15 – The relative formation of four complex molecules in $\text{CH}_4:\text{H}_2\text{O}\sim 3:1$ and $1:2$ ice mixtures (stars and diamonds, respectively) with respect to the initial CH_4 ice abundance as a function of UV fluence at 20 K.

The derived photodesorption yield is similar, within a factor of three, to the yields determined previously for CO , CO_2 , H_2O and CH_3OH (Öberg et al. 2009b,a, Chapter 10), confirming the assumption of a comparable photodesorption yield for all ices with strong UV absorptions (Chapter 12).

11.3.7 NH_3 and CH_4 photodestruction

Figure 11.18 shows the normalized and log-transformed loss of NH_3 ice as a function of fluence for different ice mixtures. In contrast to Fig. 11.17 the ices are thick (~ 50 ML) and the fluence scale short to ensure that bulk processes dominate the ice loss, rather than photodesorption of surface molecules. The measured photodestruction rates for NH_3 during the first 4×10^{16} photons cm^{-2} are reported in Table 11.1 for pure NH_3 , $\text{NH}_3:\text{H}_2\text{O}$ 1:1 and 1:4, $\text{NH}_3:\text{CH}_4$ and $\text{NH}_3:\text{CO}_2$ ice mixtures.

The photodissociation rate for pure NH_3 ice is measured to be 1.0×10^{-18} cm^2 averaged over the wavelength range of the lamp. This is an order of magnitude lower than the measured gas phase photodesorption cross section (van Dishoeck 1988). A similar discrepancy was previously found for CH_3OH , indicating that fast recombination following photodissociation is a general feature of ice photolysis. The new NH_3 ice photodissociation rate is however a factor of 8 higher than previously measured for a thick $\text{NH}_3:\text{N}_2$ 1:10 ice mixture, which is probably the most comparable measurement to the present one, since all previous photodissociation measurements are for thick ices and thick pure ices (of 1000 ML or more) suffer from optical depth effects (Cottin et al. 2003). Furthermore,

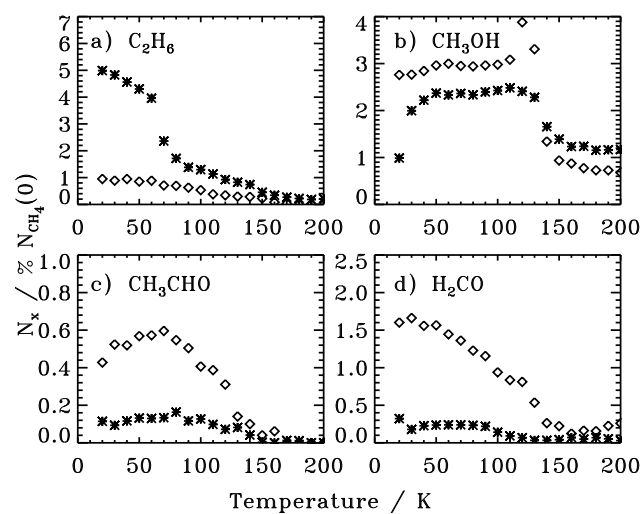


Figure 11.16 – The relative evolution of four complex molecules in $\text{CH}_4:\text{H}_2\text{O}\sim 3:1$ and $1:2$ ice mixtures (stars and diamonds, respectively) as a function of temperature during warm-up.

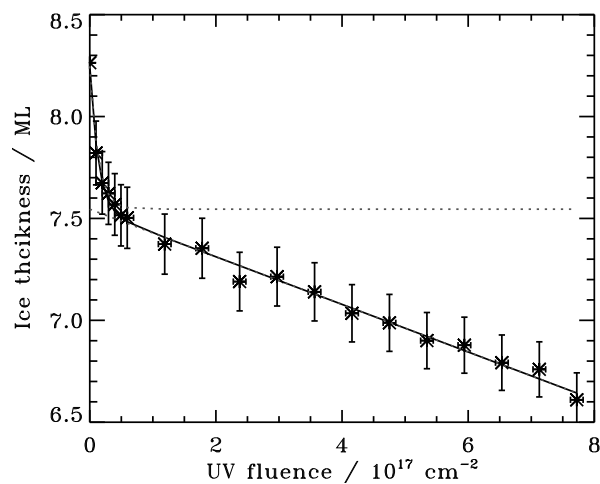


Figure 11.17 – The loss in NH_3 (stars) ice due to bulk dissociation (exponential part) and surface photodesorption (linear part). The combined fit is plotted with a solid line and the linear and exponential parts are overplotted with dotted lines.

Cottin et al. (2003) measured the photodissociation yield for an order of magnitude higher fluence, when back reactions become important; if the destruction cross section is measured over 2.3×10^{17} photons cm^{-2} , rather than just the initial few 10^{16} cm^{-2} , it would appear to be the same as measured by Cottin et al. (2003) within the experimental uncertainties. The higher photodissociation yield measured here should thus be more accurate, even though the precision of the measurements by Cottin et al. (2003) was higher.

The initial NH_3 photodestruction rate is indistinguishable in the $\text{NH}_3:\text{H}_2\text{O}$ 1:1 mixture, the $\text{NH}_3:\text{CH}_4$ 2:3 mixture and the pure NH_3 ice. At higher fluences there is still

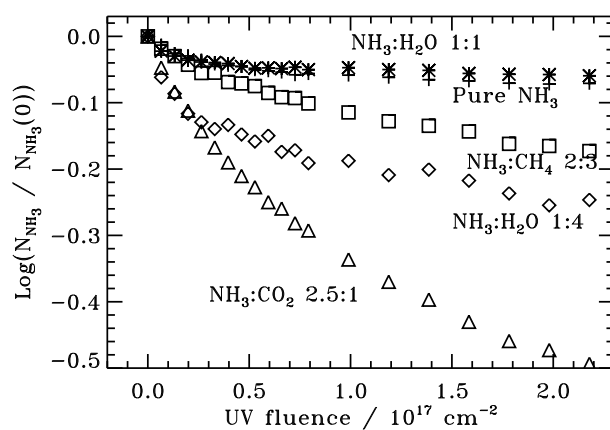


Figure 11.18 – The log-transformed normalized photodestruction rate of pure NH_3 (stars), $\text{NH}_3:\text{H}_2\text{O}$ 1:1 (crosses), $\text{NH}_3:\text{CH}_4$ 2:3 (squares), $\text{NH}_3:\text{CO}_2$ 2.5:1 (triangles) and $\text{NH}_3:\text{H}_2\text{O}$ 1:4 (diamonds) ice.

no measurable difference between the NH_3 photodissociation in pure NH_3 ice and in the $\text{NH}_3:\text{H}_2\text{O}$ mixture, while more NH_3 is being destroyed in the $\text{NH}_3:\text{CH}_4$ ice mixture. This difference suggests an efficient chemistry in the $\text{NH}_3:\text{CH}_4$ ice, which slows down the reformation of NH_3 from photodissociation fragments.

The initial photodestruction is significantly higher in the $\text{NH}_3:\text{CO}_2$ 2.5:1 and the $\text{NH}_3:\text{H}_2\text{O}$ 1:4 ice mixtures compared to pure NH_3 ice (the quoted uncertainties in Table 11.1 include the systematic uncertainties, the fit uncertainties are $\sim 0.2 \times 10^{-18} \text{ cm}^2$). In addition the destruction rate in the $\text{NH}_3:\text{CO}_2$ ice does not slow down with UV fluence. The higher initial photodestruction rate suggests an additional destruction mechanism to photodissociation, such as UV induced acid-base chemistry, i.e. NH_3 is both destroyed directly by the UV irradiation through photodissociation and indirectly through proton transfer from other photoproducts. This is the logical explanation for the high destruction rate in the $\text{NH}_3:\text{CO}_2$ ice mixture. The high rate in the 4:1 $\text{H}_2\text{O}:\text{NH}_3$ ice may also be due to a slower diffusion rate in a H_2O -rich ice, which limits back reactions. Both alternatives are discussed below together with new experiments that will constrain the relative importance of the two mechanisms.

None of this behavior is observed for CH_4 photodestruction in a similar set of ice mixtures (Fig. 11.19). Except for a 50% lower photodestruction cross section in the $\text{CH}_4:\text{NH}_3$ mixture, all CH_4 cross sections are $\sim 2.5 \times 10^{-18} \text{ cm}^2$, averaged over the wavelength range of the lamp, which is a factor of three higher than previously reported by Gerakines et al. (1996) and a factor of five lower than the gas phase value (van Dishoeck 1988). The factor of two smaller discrepancy between ice and gas phase CH_4 compared to the NH_3 case, is consistent with the expected higher volatility of $\text{CH}_2/3$ relative to NH_2 ; the faster diffusion of $\text{CH}_2/3$ should reduce the importance of immediate back reactions.

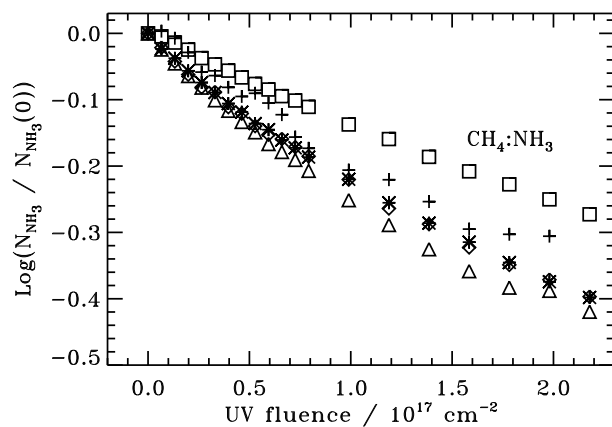


Figure 11.19 – The log-transformed normalized photodestruction rate of pure CH₄ (stars), CH₄:H₂O 3:1 (crosses), CH₄:NH₃ 3:2 (squares), CH₄:CO₂ 2:1 (triangles) and CH₄:H₂O 1:2 (diamonds) ice.

11.4 Testing complex ice formation in astrophysical ice equivalents

The comparison between photolysis of pure and binary mixtures shows that the binary reaction products are consistent with combining the pure reaction schemes with a few bridging reactions. In tertiary ice mixtures and in a four-component astrophysical ice analogue, the products are therefore expected to be consistent with the products from the binary mixtures, with some new bridging reactions combining e.g. the CH₃NH₂ and HCOOH products to form NH₂CH₂COOH in a NH₃:CH₄:CO₂ ice.

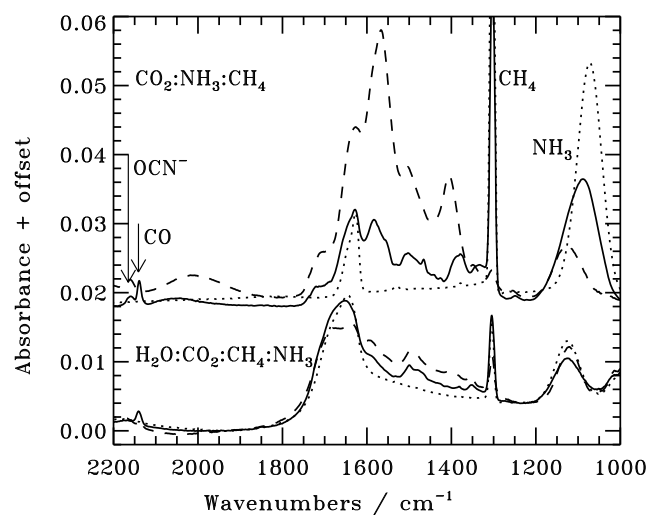


Figure 11.20 – Infrared spectra of an astrophysical ice equivalent and the NH₃:CO₂:CH₄ ice mixture before irradiation at 20 K (dotted line), following photolysis at 20 K (solid line) and after warm-up to 100 K (dashed line).

The RAIR spectra following photolysis of these ice mixtures are complicated and few of the products can be quantified spectroscopically (Fig. 11.20). Some attempts to assign peaks around $1500\text{--}1700\text{ cm}^{-1}$ have been made in previous studies following photolysis of comparable ice mixtures (Muñoz Caro & Schutte 2003), but this is not pursued here. Instead the carriers of bands outside of the $1500\text{--}1700\text{ cm}^{-1}$ spectral region, which can be securely assigned, are quantified using RAIRS. More complex products are then investigated through TPD experiments. No experiments resulted in any remaining residue after heating to room temperature as was observed in some previous experiments on thicker ices and after higher UV fluences (Greenberg 1983; Schutte & Khanna 2003).

11.4.1 Quantification of photolysis through RAIRS

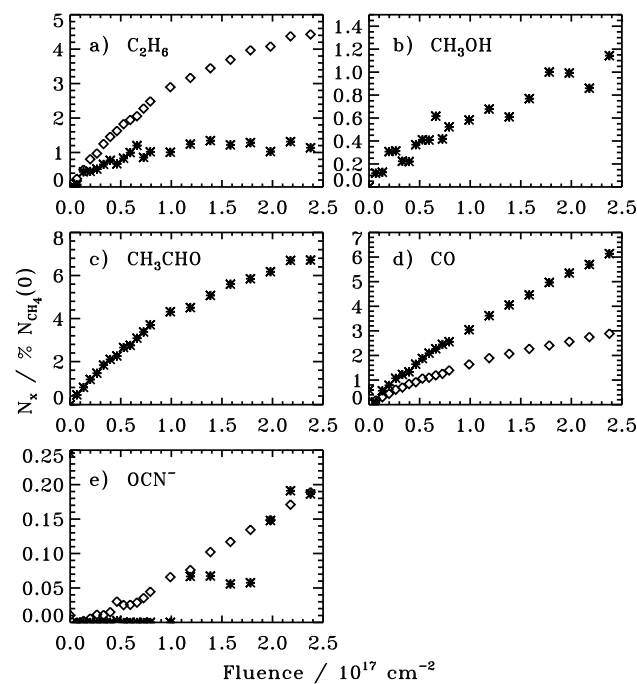


Figure 11.21 – The relative evolution of five photoproducts with respect to the initial CH_4 ice abundance in a $\text{H}_2\text{O}:\text{CO}_2:\text{NH}_3:\text{CH}_4$ 100:20:8:12 astrophysical ice equivalent (stars) and three molecules in a $\text{CO}_2:\text{NH}_3:\text{CH}_4$ ice mixture (diamonds) as a function of fluence at 20 K.

Despite the complexity of the spectra C_2H_6 , CH_3OH , CO and OCN^- formation can be identified in the astrophysical ice equivalent ($\text{H}_2\text{O}:\text{CO}_2:\text{NH}_3:\text{CH}_4$ 100:20:8:12) and in a tertiary $\text{CO}_2:\text{NH}_3:\text{CH}_4$ 1:1:1 ice mixture, through the same spectral features as in the binary ice mixtures. CH_3CHO probably forms as well though there are alternative

nitrogen-bearing carriers of the 1350 cm⁻¹ band. A comparable amount of OCN⁻ forms in both ice mixtures with respect to the CH₄ content in the ice, but the initial formation rate is lower in the H₂O-rich ice. The C₂H₆ formation is significantly reduced in the H₂O-rich ice compared to the tertiary ice mixture, suggesting that most of the CH₃ radicals react with other radicals than CH₃ in the H₂O-rich matrix forming some of the observed CH₃OH and possibly CH₃CHO.

Table 11.3 lists the formation cross sections for all detected photoproducts with known band strengths in the quantified experiments. These cross sections have a physical meaning for species that form directly through photodissociation, such as CO. For the other molecules it is simply a convenient measure of the initial photoproduction rate – the cross sections are calculated by fitting a line to the growth curves during the first 4 × 10¹⁶ photons cm⁻². This growth regime should only be marginally affected by back-reactions, except for the fast initial recombination reactions immediately following photodissociation. The cross-sections are listed with respect to initial CH₄, NH₃ and CO₂ abundances where relevant, i.e. where the product can form from photodissociation fragments of the molecule. The C₂H₆ formation is thus only listed with respect to the initial CH₄ abundance, while the CH₃NH₂ formation is listed with respect to both the CH₄ and the NH₃ abundances.

Table 11.3 – Cross sections with respect to the initial CH₄/NH₃/CO₂ abundances.

Experiment	Photoproduction cross sections / 10 ⁻¹⁹ cm ²						
	C ₂ H ₆	C ₂ H ₄	CH ₃ OH	CH ₃ CHO	CO	CO ₃	OCN ⁻
Pure CH ₄	3.2	0.36					
Pure CO ₂					13	5.5	
CH ₄ :NH ₃	4.2	0					
CH ₄ :CO ₂	7.7	0.6	2.4/-/4.3	0.34/-/0.62	14	-/0.5	
CH ₄ :H ₂ O 3:1	5.0	0.30	1.1/-/	0.27/-/			
CH ₄ :H ₂ O 1:2	2.8	<0.92	10/-/	1.9/-/			
NH ₃ :CO ₂					3.0		-/0.02/0.05
CH ₄ :NH ₃ :CO ₂	3.8				2.2		-/0.03/0.03
Astro mix	2.0		0.83/-/0.33	3.7/-/1.5	1.5		-/0/0

The initial formation rate of C₂H₆ is constant between the different experiments within a factor of three. In contrast the C₂H₄ rate is below the detection limit of ~ 10⁻²⁰ cm² in the CH₄:NH₃ mixture and the analogs and the rate thus changes by an order of magnitude.

The CH₃OH formation rate varies by an order of magnitude as well with respect to the initial CH₄ abundance in the different mixtures, indicating that the formation rate is dominated by the availability of OH radicals in the ice under most conditions, rather than the availability of CH₃. It is however also reduced in the analogue where H₂O ice is very abundant; H₂O may be too abundant in this case, caging any formed CH₃ and OH radicals from diffusing through the ice.

The CO production with respect to the CO₂ content is not affected by the presence of CH₄ and NH₃. It is however reduced by an order of magnitude in the NH₃-containing ices where acid base chemistry is feasible, i.e. the tertiary ice mixture and the analogue.

In contrast the CO₃ formation rate is reduced by an order of magnitude between the pure CO₂ ice and all other ice mixtures.

There are thus some significant quantitative differences between the binary ices and the astrophysical ice mixture analogue, which are difficult to predict without a quantitative model that takes into account the effects of acid-base chemistry and different diffusion barriers in different kinds of ices. Nevertheless, the fact that the expected photoproducts are formed in the tertiary ice and the analogue suggests that the initial hypothesis on the reaction schemes for these ices is correct; i.e. the chemistry consists of the binary ice reactions together with bridging reactions resulting in the formation of more complex molecules. Larger molecules should thus be present in the tertiary and analogue mixtures. This is the topic of the next section.

11.4.2 TPD experiments

This section investigates the TPD curves of the photolyzed astrophysical ice equivalent H₂O:CO₂:NH₃:CH₄ 100:20:12:8, together with TPD curves of five other photolyzed ice mixtures. The aim is to constrain which complex molecules form abundantly in the astrophysical ice equivalent by investigating the mass signals at each desorption peak and searching for similarities and differences between the different experiments.

The ices employed for comparison are the NH₃:CO₂ 1:1, NH₃:CH₄ 1:1, NH₃:CO₂:CH₄ 1:1:1, NH₃:CO₂:H₂O 1:1:1 and H₂O:CO₂:CH₄ 1:1:1 mixtures. All mixtures contain similar amounts of NH₃, CH₄ and CO₂ ice initially, within a factor of two, except for the analogue. All TPD curves are scaled by the same factor and the resulting TPD curves thus reflect the different formation efficiencies of different products in different ice mixtures.

Figures 11.22–11.24 present TPD curves for the nine *m/z* signals, which together contain all desorption peaks observed in the entire set of experiments. The nine *m/z* are 27, 29, 31, 41, 43, 45, 59, 60 and 61, which trace C₂H_{4/6} (27, 29), HCN (27), CH₃NH₂ (27, 29, 31), H₂CO (29), CH₃OH (29, 31), NH₂OH (31), CH₃CN (41), HNCO (43, 27), HCOOH (29, 45), CH₃COOH (45, 60), NH₂COOH (45, 61), NH₂CH₂COOH (29, 45, 59), CH₃NH₂COOH (29, 45, 60), H₂CO₃ (45, 61). *m/z* with contributions from the original ice components are purposefully avoided, i.e. *m/z*=12–18, 28 and 44, since desorption of the original ice components tend to dominate these mass signals.

The ices are heated at most to 230 K, because of experimental constraints, at which point ices are still desorbing. The desorption peaks are analyzed sequentially starting with this desorption feature around 230 K and then proceeding to lower temperatures. The resulting assignments to the desorption peaks are summarized in Table 11.4.

The 230 K desorption peak in Figs. 11.22–11.24 is present in the NH₃:CO₂:CH₄ mixture, but not in the H₂O:NH₃:CO₂ mixture, while the TPD was terminated at lower temperatures in the other experiments. The carrier of the peak must therefore contain a CH_x group. In the NH₃:CO₂:CH₄, it is present for all investigated *m/z*, including *m/z*=60 and 61. The high desorption temperature suggests a compound which exists as a salt in the ice. There is no infrared features left in the NH₃-free mixture above 200 K or in the CH₄:NH₃ mixture above 150 K and thus the molecule must contain nitrogen and a CO_x group. The

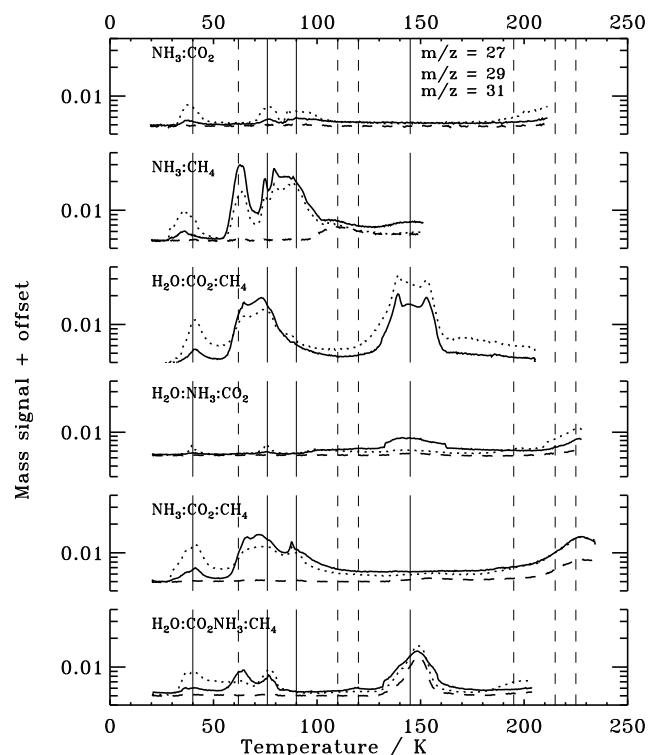


Figure 11.22 – TPD curves following photolysis of six ice mixtures for $m/z = 27$ (solid), 29 (dotted) and 31 (dashed). The thin solid lines mark the approximate desorption temperatures of CH₄, CO₂, NH₃ and H₂O. The thin dashed lines mark the desorption temperatures of different photolysis products, visible in at least one of the TPD experiments.

strong $m/z=43$, 45 and 46 peaks are indicative of CH₂COH and COOH functional groups. Glycine NH₂CH₂COOH and its structural isomer CH₃NHCOOH (CH₂COOH = 59 amu, NHCOOH = 60 amu, CH₂COH/NHCO = 43 amu, COOH=45 amu) are thus the most probable carriers though additional experiments, which include $m/z=75$ are needed to confirm the identification.

A second molecule, which does not contain a CH_x group, also desorbs around this temperature, since there is a desorption peak present at 225 K in the H₂O:NH₃:CO₂ mixture, consisting of $m/z=27$, 29, 31, 43, 45 and 46, but no 59, 60 or 61. NH₂CHO fits this mass pattern, but a new CO₂:NH₃ experiment is required to test whether the desorption is present there as well. HCOOH in its salt form is another option, which explains some of the observed mass signals.

The next desorption peak, working backwards, is at 215 K and contains $m/z=61$, but not 59 or 60 in both the H₂O:NH₃:CO₂ and NH₃:CO₂:CH₄ mixtures. $m/z=29$ and 45 are also prominent. This is indicative of NH₂COOH desorption (NH₂COOH = 61 amu,

11.4 TESTING COMPLEX ICE FORMATION IN ASTROPHYSICAL ICE EQUIVALENTS

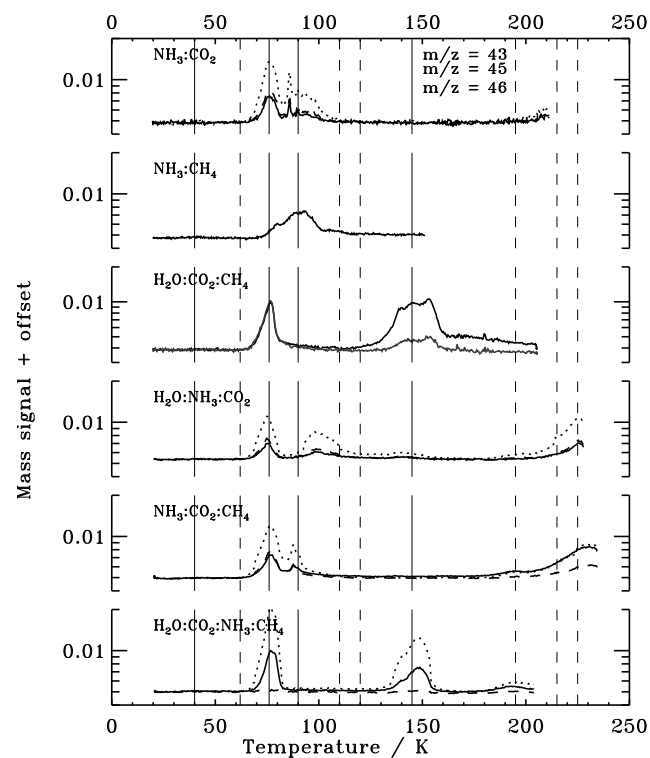


Figure 11.23 – TPD curves following photolysis of six ice mixtures for $m/z = 43$ (solid), 45 (dotted) and 46 (dashed). The thin solid lines mark the approximate desorption temperatures of CH_4 , CO_2 , NH_3 and H_2O . The thin dashed lines mark the desorption temperatures of different photolysis products, visible in at least one of the TPD experiments.

$\text{COOH} = 45$ amu, $\text{COH} = 29$ amu).

The desorption peak at 195 K is the first to be investigated that is certainly present in the astrophysical ice equivalent in the bottom panel in Figs. 11.22–11.24. It is also apparent in the $\text{NH}_3:\text{CO}_2:\text{CH}_4$ experiment with $m/z=60$, but in no other experiments. The absence in the $\text{H}_2\text{O}:\text{NH}_3:\text{CO}_2$ ice mixture is indicative of the molecule containing a CH_x group, while the absence in the N-free ice mixture advocates a molecule containing nitrogen or an acid, which requires the presence of NH_3 to exist in its ion form and thus desorbs at this high temperature. These facts and the mass pattern fits CH_3COOH and no other considered species.

H_2O desorbs at ~ 145 K. This is accompanied with significant co-desorption of $m/z \leq 46$ in the astrophysical ice equivalent and in the $\text{H}_2\text{O}:\text{CO}_2:\text{CH}_4$ ice mixture, though the mass signals are different. In the astrophysical ice the $m/z=45$ signal is stronger than the $m/z=43$ signal, while the relation is the opposite in the nitrogen free mixture. Both peaks have multiple possible carriers, but the $\text{H}_2\text{O}:\text{CO}_2:\text{CH}_4$ peak must be dominated by

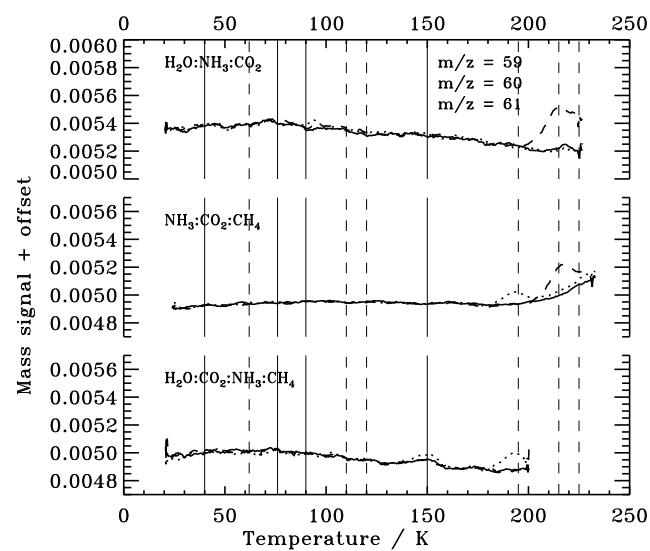


Figure 11.24 – TPD curves following photolysis of six ice mixtures for $m/z = 59$ (solid), 60 (dotted) and 61 (dashed). The thin solid lines mark the approximate desorption temperatures of CH₄, CO₂, NH₃ and H₂O. The dashed lines mark the desorption temperatures of different photolysis products, visible in at least one of the TPD experiments.

a C₂H_xO type species, while the peak in the astrophysical ice equivalent has a main carrier with a CO₂-group such as HCOOH.

The astrophysical ice equivalent and the CH₄:NH₃ ice mixture contain a peak at ~120 K. The lack of any m/z above 27 suggests that HCN is the carrier – HCN desorbs with NH₃ in the NH₃:CH₄ mixture from the RAIRS. Next, a desorption peak at 110 K is most obvious in the CH₄:NH₃ ice mixture and its mass pattern with $m/z=27-31$ makes its assignment to CH₃NH₂ secure.

There is no co-desorption with NH₃ in the astrophysical ice equivalent. The next peak at ~76 K is due to co-desorption with CO₂, which contains no obvious evidence for desorption of complex species. Finally the main C₂H₄/6 desorption peak at ~62 is present in all CH₄ containing ice mixtures.

There is no separate desorption peak for HNCO in any of the experiments, which is at first glance surprising since OCN⁻ is formed according to the RAIR spectra. Also according to the RAIR spectra, OCN⁻ starts to desorb around 200 K, and this temperature region does contain m/z signals of 28, 26 and 43. OCN⁻/HNCO must thus desorb together with other species at this temperature. It probably explains the strong $m/z=43$ signal at this time; while NH₂CH₂COOH may contribute to $m/z=43$, a rather awkward dissociation is required to form it and OCN is a more likely main contributor.

The (tentative) assignments of all desorption peaks are summarized in Table 11.4. TPD experiments following ice photolysis thus provide ample evidence for a complex NH₃ based chemistry in NH₃-containing ice mixtures up to the formation of simple amino

Table 11.4. The TPD detected species in key ice mixtures with H₂O:CO₂:CH₄:NH₃.

Temp. (K)	<i>m/z</i>	Assignment
62	27, 30, 29	C ₂ H ₄ , C ₂ H ₆
76	varied	CO ₂ co-desorption
90	varied	NH ₃ co-desorption
110	31, 29, 27	CH ₃ NH ₂
120	27	HCN
145	varied	H ₂ O co-desorption
195	45, 43, 47, 60	CH ₃ COOH ion
215	61, 45, 46, 31	NH ₂ COOH ion
225	45, 43, 46	NH ₂ CHO (+HCOOH) ion
230	60, 59, 45, 43, 46	NH ₂ CH ₂ COOH+CH ₃ NHCOOH ions (+HNCO)

acids, such as glycine. TPD curves provide little quantitative information, however and no information on when these species form during photolysis.

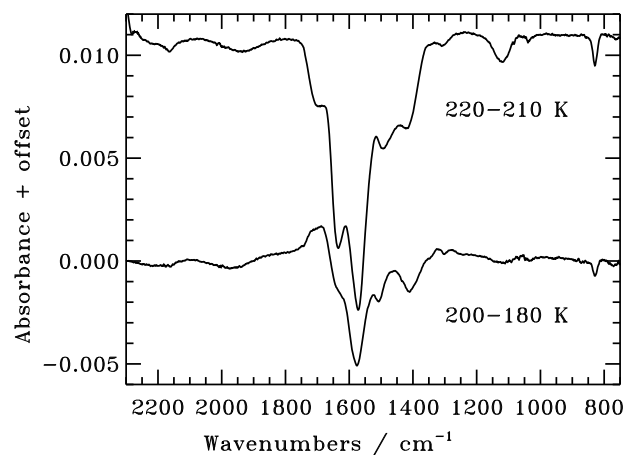


Figure 11.25 – Infrared difference spectra of the NH₃:CO₂:CH₄ ice mixture during warm-up, where negative peaks indicate destruction of the carrier in the temperature interval.

The TPD curves suggest that inspecting difference spectra from before and after specific desorption peaks may result in the assignment of some infrared peaks and the derivation of the final abundance of the complex molecule in question. Figure 11.25 shows the difference spectra of the NH₃:CO₂:H₂O mixture between 220 and 210 K and between 200 and 180 K. According to the TPD curves two different carriers are desorbing at these temperatures. Yet the difference spectra share several bands, indicating that some of the changes in the RAIRS are due to ice re-structuring, such as dissolution of the salt networks, rather than desorption. Difference spectra during desorption are thus not very useful for NH₃:CO₂-containing ice mixtures when trying to assign RAIRS features to complex molecules.

Modeling the ice chemistry in the simpler ice mixtures and then using these models to predict the chemistry in astrophysical ice analogues thus remains the best option for quantifying the complete chemistry of the H₂O-rich ice phase during star formation.

11.5 Discussion

11.5.1 Importance of acid-base chemistry in NH₃:X ice mixtures

The photodestruction rate of pure NH₃ and of NH₃ in different ice mixtures differs by a factor of four after a low fluence and by an order of magnitude after an equivalent photon exposure to a million years in a cloud core, i.e. $\sim 3 \times 10^{17}$ photons cm⁻² (Shen et al. 2004). In contrast the CH₄ photodissociation rate increases by at most 50% between the pure ice and a similar set of ice mixtures as investigated for NH₃.

There are a number of processes that can affect the effective photodissociation cross sections in ices of which the diffusion and escape rates of radicals have been shown to be important previously (Chapter 10). The diffusion rate can be increased by increasing the ice temperature and decreased by the presence of a strongly binding ice such as H₂O. An increased diffusion rate should increase the recombination rate. An increasing temperature may also result in desorption of radicals, which has the opposite effect of decreasing the recombination rate, which is probably why the effective CH₃OH photodissociation rate increases with temperature (Chapter 10). The lowered diffusion rate in a H₂O-rich ice may explain why the NH₃ photodissociation cross section is higher in the H₂O:NH₃ 4:1 mixture compared to pure NH₃ ice. A similar effect would be expected for CH₄. This is not observed, but may be due to the fact that the highest H₂O concentration investigated is H₂O:CH₄ 2:1 and a 5:1 experiment is required to investigate this further.

The increased photodestruction rate of NH₃ in the H₂O ice may also be due to a photo-induced acid-base chemistry where H₂O or a H₂O:NH₃ photoproduct acts as a weak acid. Acid-base chemistry is the only explanation for the extremely efficient indirect photodestruction of NH₃ in a CO₂ ice mixture. There NH₃ must be lost both by photodissociation and by proton transfer from photoproducts, such as HCOOH and H₂CO₃, to form NH₄⁺. Acid base chemistry in NH₃ and CO₂ containing ices also explains the high desorption temperatures of several of the complex molecules, e.g. NH₂COOH, CH₃COOH and possibly NH₂CH₂COOH/CH₃NHCOOH, since salts form stronger bonds than the covalent bonds between the neutral molecules in the ice.

The impact on the chemical pathways of this proton transfer is not clear. The tentatively detected complex molecules in the NH₃:CO₂:X mixtures can all be qualitatively explained by radical-radical reactions, e.g. NH₂+CH₂+COOH to form NH₂CH₂COOH, followed by proton loss to NH₃ to form NH₄⁺. This indicates that the acid-base chemistry does not effect the formation pathways of species, but only the final form of the products and therefore their desorption temperatures. The predicted high desorption temperatures of most nitrogen-containing organics may explain why no glycine has been detected in space yet – it is probably present in the gas phase in a very small region around protostars.

11.5.2 Photodissociation branching ratios

H₂O, CH₄ and NH₃ all photodissociate through the loss of one or multiple hydrogen atoms or a hydrogen molecule, while CO₂ exclusively photodissociates into CO+O in the gas phase (van Dishoeck 1988). The H₂O and NH₃ photodissociation branching ratios cannot be quantified in the pure ices because of the lack of secure product detections and band strengths. Their gas phase values are however well known and should be valid in the solid state as well. The gas phase CH₄ photodissociation branching ratio into CH₃ and CH₂ is more controversial and experiments have suggested values between 5:1 and 1:1 (Romanzin et al. 2008).

Following CH₄ photolysis in the pure ice, both C₂H₆ and C₂H₄ are detected. The growth curve of C₂H₄ contains a small fluence delay, but it is not large enough to infer that C₂H₄ is a second generation product as e.g. CH₃CH₂OH seems to be in the CH₄:H₂O ice. Thus the initial growth of both C₂H₄ and C₂H₆ is assumed to be caused by CH₃+CH₃ and CH₂+CH₂ radical reactions. Further assuming that the diffusion barriers of CH₃ and CH₂ are comparable, the CH₄ branching ratio can be constrained from the initial C₂H₆ and C₂H₄ production rate, which is ~9:1. Since each reaction requires two radicals, the dissociation branching ratio is inferred to be ~3:1.

The product ratios during UV irradiation will also depend on the relative radical diffusion barriers. Quantifying these barriers requires, however, a model that simultaneously considers all possible reactions pathways.

11.5.3 Radical diffusion: dependence on H₂O content

Diffusion data can also be extracted by monitoring the further formation of complex molecules during warm-up after the UV lamp has been turned off. This is most obvious when comparing the CH₃OH and CH₃CHO formation in a H₂O-poor and a H₂O-rich H₂O:CH₄ ice mixture during warm-up, following irradiation at 20 K. In the H₂O-poor ice mixture CH₃OH forms during warm-up, but almost no CH₃CHO. In the H₂O-rich ice the situation is the opposite. In both ices more OH than CHO radicals are expected to form, since OH is a direct photodissociation product of H₂O. The growth of CH₃OH in the H₂O-poor ice mixture, where diffusion is fast, is thus expected. The enhanced growth of CH₃CHO in the H₂O-rich ice is best explained by a slower diffusion rate of OH in this ice mixture, because of the hydrogen-bonding environment, which allows the more volatile CHO radical to react with the available CH₃ radicals before OH diffusion becomes possible. While branching ratios can be directly extrapolated from simpler to more complex ice mixtures, it is clear that adding H₂O may change the relative diffusion pattern of the involved radicals significantly and this must be further investigated as outlined below.

11.5.4 Radical-radical versus radical-molecule reactions

The CHO radical belongs to the set of species in the considered reaction schemes which form from hydrogenation and oxygenation of molecules rather than radicals, i.e. CO+H,

though photodissociation pathways from other molecules are possible as well. The formation of CO₃ and O₃ in the CO₂ ices are other examples as is the tentative evidence for HCOOH formation. Hydrogenation of CO is possible for thermalized hydrogen atoms, while hydrogenation of CO₂ is not (Watanabe et al. 2000; Bisschop et al. 2007b). The definite formation of CO₃ from CO₂+O shows that atom addition to CO₂ is possible for at least energetic atoms – whether the O needs to be energetic to react with CO₂ should be tested through irradiation of matrix-isolated CO₂ followed by warm-up. CO₂ hydrogenation may thus be important for energetic hydrogen atoms and HCOOH may form from CO₂ + H* + H.

The order of magnitude decrease in CO₃ and O₃ formation in the ice mixtures compared to the pure CO₂ ice and the far smaller effect on CO production demonstrates that radicals are preferentially hydrogenated in ice mixtures of molecules and radicals, in agreement with Hasegawa et al. (1992). A quantitative measurement of this effect would be possible if the relative production rate of HCOOH and H₂CO₃ could be determined under some specific conditions and this is being pursued.

11.5.5 Routes to complex organics in space

Chapter 10 showed that photolysis of CH₃OH and CO:CH₃OH ices results in the formation of all common C, O and H bearing complex organic species observed in star forming regions. Several of the same species form abundantly, i.e. a few percent with respect to CH₄, during photolysis of H₂O:CO₂:CH₄ ice mixtures as well. The dominating formation pathway of e.g. CH₃CHO will therefore depend on 1) the initial ice abundances and 2) the efficiency of ice mixing during warm-up. Other complex molecules, such as (CH₂OH)₂, are still expected to form solely in the CH₃OH:CO ice phase.

The N-containing organic species require NH₃ or XCN to form (a very minor route through N₂ photolysis cannot be excluded). The NH₃ is expected to reside solely in the H₂O-rich phase, while the XCN species may form in either the CO-rich or the H₂O-rich ice phases (Chapter 2). The order of magnitude higher abundances of NH₃ compared to e.g. OCN⁻ and HCN suggest, however, that formation paths of the majority of nitrogen-containing complex species should be possible to predict from the experiments on H₂O-rich ices, without simultaneous consideration of the chemistry in the CO:CH₃OH ice phase.

The pure and binary ice experiments, where the product formation is quite well understood, produce complex photoproducts in accordance with simple radical-radical and radical-molecule reaction schemes. The same complex molecules seem to form in the astrophysical ice analogue and in the binary ice mixtures it can be thought of as being composed of. Quantitative difference between the two types of mixtures highlight the importance of H₂O and its impact on the relative diffusion barriers of different radicals as discussed further below. To quantitatively test whether the analogue chemistry is consistent with predictions from the binary ice mixtures requires a complete model of the chemistry of both the binary and the analogue mixtures. Such a model should preferentially be calibrated against the better understood chemistry in the simple ice mixtures and then model the analogue based on this calibration. The predicted chemistry can then be

compared quantitatively with the growth curves in the analogue and qualitatively with the results from the TPD experiments.

Even without such a model, it is clear that substantial amounts of amino acids and amino acid-like compounds can form in NH_3 and CO_2 containing ices. The experiments also show that these large molecules can form during irradiation of astrophysically plausible ice mixtures at 20 K or due to diffusion of formed radicals during warm-up of the same ices to at most 200 K. Room temperature induced reactions are therefore not required to form such complex molecules, which is promising for the formation of large molecules in ices in space.

11.5.6 Future experiments

An accurate prediction of the complex chemistry in astrophysically realistic ice mixtures requires a number of additional experiments focusing on the impact of H_2O on the diffusion of radicals and molecules, especially CH_3 , CH_2 , NH_2 , NH , CO and HCO . This can be achieved by quantifying the changes in the chemistry of the binary mixtures investigated here when they are mixed with five times as much H_2O and then irradiated at 2–3 temperatures, e.g. 20, 40 and 60 K. Analysis of these new experiments and especially the determination of product branching ratios under different conditions will result in relative diffusion barriers and their relative dependence on the ice mixture composition. These experiments would also constrain the mechanism behind the increasing photodestruction cross section of NH_3 in a H_2O -dominated matrix.

11.6 Conclusions

There is no doubt that complex nitrogen-bearing molecules can form through photochemistry in the H_2O -rich ice observed towards protostars. The experimental quantification of this formation process is non-trivial because of overlapping infrared spectral features in astrophysical ice mixtures analogues. This difficulty was addressed by combining the quantification of a small set of photolysis products in a range of pure ices, binary ice mixtures and more complex astrophysical ice analogues, and TPD experiments constraining the formation of more complex species. The main findings from this approach are summarized below.

1. The product ratio of C_2H_6 and C_2H_4 in pure CH_4 ice implies a CH_4 photodissociation branching ratio of $\text{CH}_3:\text{CH}_2$ of 3:1, averaged over the wavelength range of the lamp.
2. In binary $\text{CH}_4:\text{NH}_3/\text{H}_2\text{O}/\text{CO}_2$ and $\text{NH}_3:\text{CO}_2$ ice mixtures the formation curves of C_2H_6 , CH_3NH_2 and CH_3OH are consistent with formation from two first generation radicals, while HCN , $\text{CH}_3\text{CH}_2\text{OH}$, CH_3CHO and OCN^- formation requires several reaction steps. This is consistent with reaction schemes, where products

form from radical-radical and radical-molecules reactions, and radicals are produced both from photodissociation of the original ice constituents and through photodissociation of first-generation photoproducts.

3. Increasing the H₂O concentration in the ice increases the diffusion barriers of hydrogen-bonding radicals relative to non-hydrogen-bonding radicals, which changes the chemical evolution of the ice.
4. NH₃ ice is both destroyed directly by UV photons through photodissociation and indirectly through proton transfer with other photoproducts. In CO₂ containing ices, the indirect acid-base NH₃ destruction path is up to an order of magnitude more important.
5. The most abundant photoproducts in the binary ices are also detected upon irradiation of a H₂O:CO₂:NH₃:CH₄ 100:20:12:8 astrophysical ice analogue. The formation rates are however different compared to most binary ices because of acid-base chemistry and the different diffusion pattern in H₂O-rich and H₂O-poor ices.
6. TPD experiments of tertiary ice mixtures show that glycine can form already at low temperatures in ices containing CO₂:NH₃:CH₄. Other detected photoproducts are NH₂CHO, CH₃COOH and NH₂COOH. All exist in salt form because of proton transfer with NH₃, which results in higher desorption temperatures than e.g. H₂O ice.

The results suggest that the information from the pure and binary ice mixture experiments can be used to predict the chemistry in astrophysical ice analogues both in the laboratory and under astrophysical conditions. Quantifying the complex N-bearing ice chemistry during star and planet formation is thus within reach.